Am J Transl Res 2014;6(3):291-301
www.ajtr.org /ISSN:1943-8141/AJTR0000225

Original Article

Engineered 3D bioimplants using elastomeric scaffold, self-assembling peptide hydrogel, and adipose tissue-derived progenitor cells for cardiac regeneration

Carolina Soler-Botija[1], Juli R Bagó[2], Aida Llucià-Valldeperas[1], Ana Vallés-Lluch[3], Cristina Castells-Sala[4], Cristina Martínez-Ramos[3], Teresa Fernández-Muiños[4], Juan Carlos Chachques[5], Manuel Monleón Pradas[3], Carlos E Semino[4], Antoni Bayes-Genis[1,6]

[1]Heart Failure and Cardiac Regeneration (ICREC) Research Program, Health Research Institute Germans Trias i Pujol (IGTP), Cardiology Service, Hospital Universitari Germans Trias i Pujol, Badalona, Spain; [2]Division of Molecular Pharmaceutics, UNC Eshelman School of Pharmacy, University of North Carolina at Chapel Hill, Genetic Medicine Building, Chapel Hill NC, USA; [3]Center for Biomaterials and Tissue Engineering, Universitat Politècnica de València, Valencia, Spain; [4]Department of Bioengineering, IQS-School of Engineering, Ramon Llull University, Barcelona, Spain; [5]Department of Cardiovascular Surgery, Pompidou Hospital, Paris, France; [6]Department of Medicine, Autonomous University Barcelona, Spain

Received March 13, 2014; Accepted April 18, 2014; Epub May 15, 2014; Published May 30, 2014

Abstract: Contractile restoration of myocardial scars remains a challenge with important clinical implications. Here, a combination of porous elastomeric membrane, peptide hydrogel, and subcutaneous adipose tissue-derived progenitor cells (subATDPCs) was designed and evaluated as a bioimplant for cardiac regeneration in a mouse model of myocardial infarction. SubATDPCs were doubly transduced with lentiviral vectors to express bioluminescent-fluorescent reporters driven by constitutively active, cardiac tissue-specific promoters. Cells were seeded into an engineered bioimplant consisting of a scaffold (polycaprolactone methacryloyloxyethyl ester) filled with a peptide hydrogel (PuraMatrix™), and transplanted to cover injured myocardium. Bioluminescence and fluorescence quantifications showed *de novo* and progressive increases in promoter expression in bioactive implant-treated animals. The bioactive implant was well adapted to the heart, and fully functional vessels traversed the myocardium-bioactive implant interface. Treatment translated into a detectable positive effect on cardiac function, as revealed by echocardiography. Thus, this novel implant is a promising construct for supporting myocardial regeneration.

Keywords: Cardiac regeneration, subcutaneous ATDPCs, self-assembling peptide hydrogel, elastomeric membrane, RECATABI

Introduction

Acute myocardial infarction (MI) is a leading cause of mortality all over the world that occurs due to interruption of the blood supply to the heart [1]. As a consequence, a massive loss of cardiomyocytes occurs and a fibrotic scar is formed, leading to non-contractile myocardium and enlargement of the left ventricle [2, 3]. Given the limited regenerative capacity of the myocardium after ischemic damage [4], cellular cardiomyoplasty has emerged as a promising therapeutic strategy [5]. Although preclinical studies and clinical trials of cell transplantation for cardiac regeneration have demonstrated certain beneficial effects and safety, these treatments were not as effective as expected due to poor cell retention and survival in the contracting myocardium [6-14]. Aside from choosing the optimal cell type for cardiac regeneration, the ideal route of cell delivery and the optimal dose remain controversial [15].

New strategies have emerged to circumvent these difficulties, such as the development of cardiac tissue engineering and myocardial bioprosthesis [16]. In myocardial bioprosthesis, functional cardiac tissue replacements are created from biological and synthetic materials, often in combination with regenerative cells and other biochemical factors [17-20]. The goal is to generate a suitable environment for cell

survival within the hostile conditions of the ischemic myocardium, and to differentiate these cells into cardiac or endothelial lineages with the ultimate purpose of regenerating the damaged myocardium. Accordingly, the RECATABI (Regeneration of Cardiac Tissue Assisted by Bioactive Implants) consortium has designed and produced novel bioactive implants using innovative biomaterial combinations that may improve cell delivery, survival, migration, and differentiation into newly functional myocardial tissue (http://www.recatabi.com/).

We developed a bioactive implant consisting of partially biodegradable elastomeric membranes that act as a scaffold; the membranes are filled with a self-assembling peptide hydrogel and cells with cardiac regenerative potential, subcutaneous adipose tissue-derived progenitor cells (subATDPCs) [21-24]. Here, we evaluated the effect of this novel bioactive implant on cell survival and differentiation, and analyzed tolerance and functional benefits of the implant in a mouse model of MI.

Material and methods

Isolation and culture of subATDPCs

Cells were isolated from subcutaneous adipose tissue between the skin and the sternum of patients undergoing cardiac surgery. Informed consent was obtained from all subjects, and the study protocol conformed to the principles outlined in the Declaration of Helsinki. Biopsy samples were processed and cells were isolated as described previously [25, 26]. Adhered cells were cultured to subconfluence under standard conditions (37°C and 5% CO_2).

Genetic labeling of subATDPCs with bioluminescent and fluorescent reporters regulated by the human cardiac troponin I promoter (hcTnIp) or the cytomegalovirus promoter (CMVp)

SubATDPCs were co-transduced (2×10^6 transducing units/mL, multiplicity of infection=21, 48 h) with the following lentiviral vectors: (1) CMVp-RLuc-mRFP1, which contains a chimeric construct of the *Renilla reniformis* luciferase (RLuc) reporter and monomeric red fluorescent protein (mRFP1) in a pHR lentiviral vector under transcriptional control of the CMV promoter [27], and (2) hcTnIp-PLuc-eGFP, a fusion reporter vector comprised of the *Photinus phyralis* luciferase (PLuc) and enhanced green fluorescent protein (eGFP) coding regions under the transcriptional control of hcTnIp, which is transcriptionally active in cardiomyocytes [23]. Cells expressing mRFP1 were selected by fluorescence-activated cell sorting.

Generating elastomeric membranes (microporous scaffolds)

Poly (caprolactone 2-(methacryloyloxy)ethyl ester) (PCLMA) scaffolds with spherical interconnected pores were prepared as previously described [21]. Briefly, the monomeric solution was mixed with 1 wt% of benzoin (98%, Scharlau) as photo-initiator and 2 wt% of ethyleneglycol dimethacrylate (98%, Aldrich) as cross-linker, injected into a porogen template obtained by sintering poly(methyl methacrylate) microspheres 90 ± 10 μm in diameter (dp 300, Colacryl), polymerized for 24 h under ultraviolet light, and post-polymerized for another 24 h in an oven at 90°C. After polymerization, the porogen was eliminated by dissolution with acetone (Scharlab). The acetone was then slowly exchanged for water, and the resulting scaffolds were dried under vacuum. PCLMA scaffolds were cut into 3 × 3 × 0.5 membranes and sterilized with gamma radiation before cell seeding.

Development of the bioactive implants: cell-seeded elastomeric membranes prefilled with RAD16-I self-assembling peptide

The self-assembling peptide RAD16-I (PuraMatrix™ 1% (w/v), BD Biosciences) was used to fill the pores in the PCLMA scaffolds. Prior to use, RAD16-I was sonicated for 30 min at 25°C, applying 30 W to reduce its viscosity (Bandelin). The elastomeric membranes were then embedded in a 0.15% solution of RAD16-I nanofiber peptide using a syringe as a vacuum system. Next, 0.5×10^6 subATDPCs suspended in 10% sucrose were seeded inside the construct and incubated with soft shaking for 30 min. Sucrose solution without cells was added to the control membranes. Then, 160 μL of culture medium was used to increase the ionic strength of the system and thus to induce the self-assembly of the peptides into nanofibers. Finally, the constructs were cultured under standard conditions (37°C and 5% CO_2) for one day before implantation.

MI model and bioimplant delivery

A total of 25 female severe combined immunodeficiency mice (20-25 g; Charles River Laboratories, Inc.) were used for this study. The animals were randomly assigned to one of the following four groups: (1) bioimplant implantation and no MI induction (the sham group, n=6), (2) MI induction and no bioimplant (the control-MI group, n=5), (3) MI induction and scaffold implantation (the MI-scaffold group, n=5), and (4) MI induction and bioimplant implantation (the MI-bioimplant group, n=9).

MI was induced as previously described [25]. Briefly, each animal was intubated and anesthetized with a mixture of O_2/isoflurane and mechanically ventilated. The heart was exposed and the left anterior descending coronary artery was permanently occluded. Bioimplants or scaffolds were then implanted using synthetic surgical glue (Glubran®2) on the healthy myocardium. Four weeks post-implantation, hearts were arrested in diastole with cardioplegic solution (68.4 mM NaCl, 59 mM KCl, 11.1 mM glucose, 1.9 mM $NaHCO_3$, 29.7 mM 2,3-butanedione monoxime, 1000 U heparin), excised, fixed, cryopreserved in 30% sucrose in phosphate-buffered saline, embedded in Tissue-Tek O.C.T. (Sakura), and snap-frozen in liquid nitrogen-cooled isopentane. Tissue blocks were stored at -80°C until sectioning. All animal handling procedures were approved by the Institutional Animal Care and Use Committee and conformed to the Guide for the Care and Use of Laboratory Animals of the Institute of Laboratory Animal Research (NIH Pub. No. 86-23, Revised 1996).

Non-invasive bioluminescence imaging (BLI) of luciferase activity and fluorescence detection in the bioimplant

For *in vivo* BLI, anesthetized mice bearing a bioimplant seeded with transduced cells were intraperitoneally injected with 150 μL of luciferin (16.7 mg/mL in physiological serum) (Caliper) for PLuc detection. The next day, animals were intravenously (tail vein) injected with 25 μL of benzyl coelenterazine (1 mg/mL in 50/50 propilene glycol/ethanol; Nanolight Technology) diluted in 125 μL for the detection of RLuc-expressing cells. Mice were monitored immediately after implantation and at 1, 2, and 3 weeks post-implantation. Fluorescence was also detected from the excised hearts immediately after sacrifice. Quantification and analysis of photons recorded and fluorescence in images were performed using the Caliper image analysis software (Caliper).

Cardiac function determination

Transthoracic echocardiography was performed under light sedation (1% isoflurane in O_2) before surgery (baseline), two days after surgery (MI), and at 4 weeks after surgery (pre-sacrifice). A digital ultrasound system (Vevo 2100 Imaging System, VisualSonics) equipped with an 18-38 MHz linear-array transducer was used to take measurements. Images were obtained in B-Mode and M-Mode in the parasternal long-axis and short-axis views. All images were acquired and measured by an investigator who was blinded to the treatment groups. Conventional functional parameters were measured, including left ventricle fractional shortening, left ventricle ejection fraction (LVEF), left ventricle anterior wall, left ventricle posterior wall, left ventricle end-diastolic dimension, and left ventricle end-systolic dimension.

Histological evaluation

Mouse hearts were transversally sliced into two segments at the ligation level. Eight serial cryosections (spaced 200 μm apart) from the apical segment were stained with Masson's trichrome. All sections were blindly examined and photographed using a SMZ 800 stereoscope (Nikon).

Immunohistochemistry

Mouse heart cryosections were incubated with primary antibodies against cardiac troponin I (cTnI; 2 μg/mL; Abcam). Sections were also incubated with RFP and GFP antibodies (2 μg/mL; Abcam) to enhance the detection of transduced cells. Nuclei were counterstained with Hoechst 33342, and results were analyzed with a Leica TCS SP2 confocal microscope.

Fluorescence angiography

Fluorescein isothiocyanate (FITC)-dextran (Sigma) was used as a fluorescent tracer of microvascular structures in bioimplants and hearts. Two hundred microliters of FITC-dextran (10

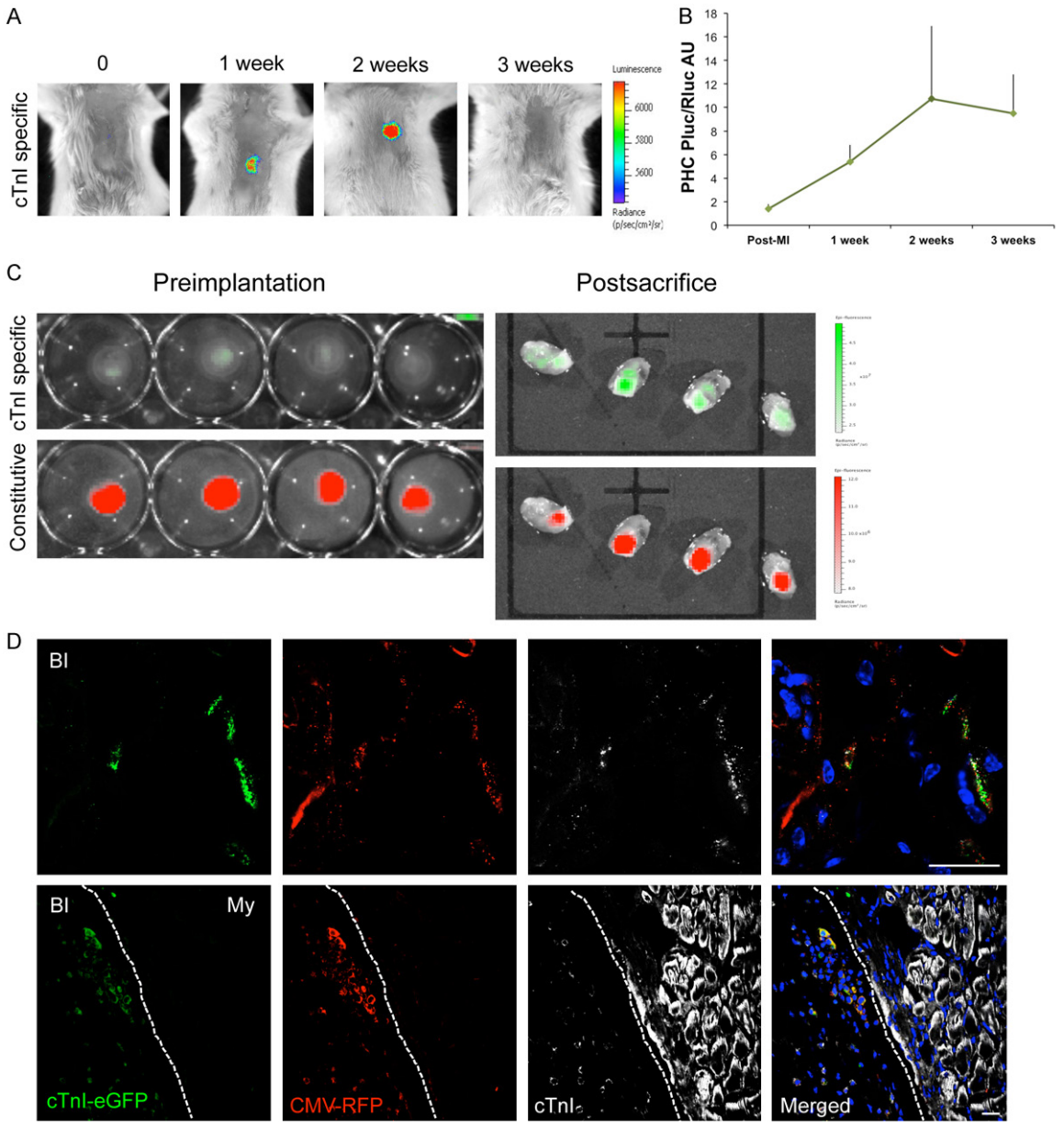

Figure 1. BLI and fluorescent evaluation of cTnI expression and survival of subATDPCs implanted over the mouse infarcted myocardium. A: Representative BLI of labeled subATDPCs within the bioactive implant displays the luciferase signal from the cell differentiation reporter (PLuc-eGFP) that is regulated by the hcTnI promoter. Images of the hcTnI-specific reporter are superimposed on black-and-white dorsal images of the recipient animal. Color bars illustrate relative light intensities from PLuc. B: Histograms of the PLuc/RLuc ratio calculated from photon fluxes recorded via BLI from bioactive implant-treated infarcted animals. C: Representative fluorescence images from subATDPCs within the bioactive implant pre-implantation and post-sacrifice over the excised hearts. Upper images show fluorescence from the cell differentiation reporter (PLuc-eGFP) regulated by hcTnIp (green). Bottom images are representative of constitutive fluorescence from the cell-number reporter (CMVp-RLuc-mRFP1; red). Color bars illustrate the relative fluorescence intensities from eGFP (green) and RFP (red). D: Immunofluorescence staining of mouse heart cross-sections shows the bioactive implant filled with human subATDPCs. Transplanted cells were detected via RFP immunostaining (red), and cTnI expression was detected with anti-eGFP (green) and anti-cTnI (white) antibodies. (BI, bioactive implant; My, myocardium). Scale bars, 20 μm.

mg/mL) were injected through the lateral tail vein of anesthetized mice 10 min before sacrifice. Laser confocal microscopy (Axio-Observer Z1, Zeiss) was used for section analysis.

Statistical analysis

The statistical significance of bioluminescence and cardiac-function parameters was evaluated via analysis of variance (factors: time and treatment) and a Greenhouse correction was applied. Results are presented as mean standard error of the mean. *P*-values<0.05 were considered significant. All analyses were performed with SPSS Statistics version 19 (IBM).

Results

SubATDPCs express hcTnI after implantation over infarcted myocardium by means of a biosynthetic bioactive implant

In these experiments, we sought to monitor cardiomyogenic lineage differentiation and survival of subATDPCs *in vivo*, using non-invasive BLI. For this purpose, cells were transduced using lentiviral vector CMVp-RLuc-mRFP1 to express the RLuc-RFP reporter under the regulation of the CMV promoter, a reporter of cell number. Then, to monitor cardiomyogenic lineage differentiation, positively transduced cells expressing RLuc-RFP were selected by fluorescence-activated cell sorting and transduced with lentiviral vector hcTnIp-PLuc-eGFP to express the PLuc-eGFP reporter under the regulation of hcTnIp. Doubly transduced cells were loaded into the bioactive implant and delivered to the infarcted area in a mouse model of MI.

Photon counts revealed an increase in the ratio between hcTnIp-regulated PLuc and CMV-regulated RLuc activities in infarcted (**Figure 1A** and **1B**) and sham-infarcted (data not shown) animals. hcTnI was expressed *de novo* as early as one week post-implantation, with expression increasing up to 9-fold at 3 weeks. Interestingly, an important RFP signal was detected in excised hearts, indicating the retention and local presence of the implanted cells after sacrifice (**Figure 1C**). In concordance with BLI, GFP was also detected, indicating hcTnI expression at the time of sacrifice. Comparisons of the GFP/RFP ratio pre-implantation and at sacrifice demonstrated a 16-fold increase in hcTnI expression.

Immunodetection of RFP in histological analyses of excised heart cross-sections revealed the presence of subATDPCs in the bioactive implant up to 4 weeks after implantation in all analyzed groups (**Figure 1D**). Additionally, to relate hcTnI gene and protein expression, immunostaining against hcTnI protein was performed in all cell-treated animals. RFP, GFP, and hcTnI proteins co-localized in implanted subATDPCs (**Figure 1D**), validating the BLI analysis and providing evidence of differentiation into the cardiac lineage. However, no implanted subATDPCs were observed in the myocardium of infarcted or sham-treated animals, indicating an absence of migration from the bioactive implant to the underlying heart.

Adaptability and vascularization of the bioimplant in the mouse model of MI

Macroscopic and histological observations of excised hearts and cross-sections demonstrated that the bioactive implants were perfectly adapted to the mouse myocardium covering the infarcted scar (**Figure 2A** and **2B**). Moreover, RFP-expressing subATDPCs were observed inside the bioactive implant and displayed the same spindle-shaped morphology observed in culture (**Figure 2C** and **2C'**). Taken together, our observations indicate that the PCLMA elastomeric membrane confers a suitable environment for subATDPC survival.

To determine whether functional vessel connections had been established between the bioactive implant and the myocardium, animals received FITC-dextran through the tail vein prior to sacrifice. The bioactive implant was fully vascularized in all cases, including control animals that did not receive cell transplants (**Figure 2D** and **2E**); the vessels were connected to the circulatory system (**Figure 2D**, arrowhead) and were functional (**Figure 2D** and **2E**).

The bioactive implant positively affects global cardiac function

To evaluate the effect of the bioactive implant on cardiac function in the mouse infarcted myocardium, echocardiographic analyses were performed. Conventional measures of global left ventricle function, such as LVEF, revealed that infarcted animals treated with the bioactive implants with or without cells presented functional improvement at sacrifice (48% and 47%, respectively) (**Table 1**, **Figure 3A** and **3B**). LVEF relative changes, expressed as differences between values post-infarction and at sacrifice, were higher in control-MI animals (-17.5%)

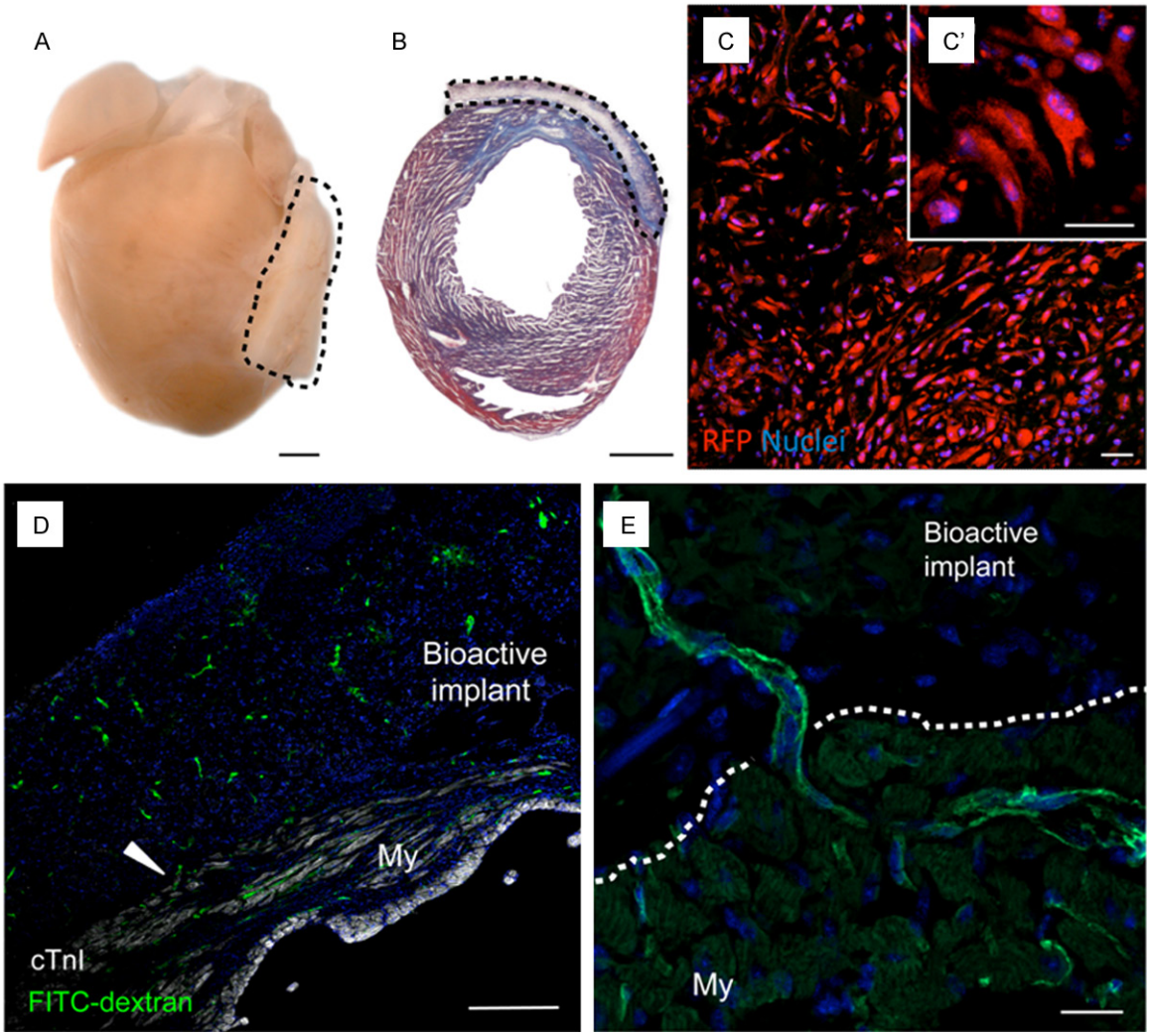

Figure 2. Adaptability and vascularization of the bioimplant in the mouse model of MI. A: Representative image of a heart excised from a bioactive implant-treated animal. Dotted lines indicate localization of the implant. Scale bars, 1 mm. B: Masson's trichrome staining in a heart cross-section reveals the presence of a myocardial scar (blue) and the good adaptability of the bioactive implant. Scale bars, 1 mm. C: Cells inside the bioactive implant three days post-implantation were detected via the constitutively active reporter CMVp-RLuc-mRFP1 (red). C': Detail of the spindle-shape morphology of subATDPCs. Scale bars, 25 μm. D and E: Functional vessel detection with FITC-dextran (green) in mice treated with subATDPCs. Arrowheads indicate a vessel connection between the mouse myocardium and the bioactive implant in a cell-treated animal. Nuclei were counterstained with Hoechst 33342. Scale bars, 20 μm and 250 μm.

than in MI-bioimplant animals (-14.1%) or in the MI-scaffold group (-13.6%) (**Figure 3C**). Analysis of variance revealed that the LVEF of cell-treated mice did not significantly differ from that of non-infarcted (sham-treated) animals (P=0.10).

Discussion

Cardiac tissue engineering and myocardial bioprosthesis have evolved over recent years as therapeutic alternatives for replacing damaged tissue after MI. These approaches propose the *in vitro* generation of artificial cardiovascular tissue platforms with similar characteristics to the heart for use as a myocardial replacement or for cell and molecule delivery [28]. Numerous materials with defined composition and properties as well as various cell types have been studied, but the optimal combination has not yet been identified.

We have generated and tested a platform consisting of partially biodegradable elastomeric membranes (PCLMA) loaded with peptide

Table 1. Cardiac function parameters

	Sham			Control-MI			MI-Scaffold			MI-Bioimplant		
	Baseline	Post-op	30 days	Baseline	Post-MI	30 days	Baseline	Post-MI	30 days	Baseline	Post-MI	30 days
AWd (mm)	0.9 ± 0.1	1.1 ± 0.2	0.9 ± 0.2	0.7 ± 0.2	0.8 ± 0.3	0.7 ± 0.2	0.8 ± 0.3	1.1 ± 0.2	0.8 ± 0.2	1.0 ± 0.3	1.0 ± 0.2	0.9 ± 0.1
AWs (mm)	1.3 ± 0.2	1.4 ± 0.4	1.2 ± 0.2	1.2 ± 0.1	1.2 ± 0.6	0.8 ± 0.2	1.0 ± 0.2	1.2 ± 0.3	1.1 ± 0.2	1.1 ± 0.4	1.4 ± 0.2	1.3 ± 0.2
PWd (mm)	1.0 ± 0.2	0.9 ± 0.1	0.9 ± 0.1	0.8 ± 0.2	0.7 ± 0.2	1.0 ± 0.2	0.9 ± 0.1	0.8 ± 0.2	1.0 ± 0.2	0.7 ± 0.1	0.9 ± 0.2	1.0 ± 0.2
PWs (mm)	1.6 ± 0.3	1.3 ± 0.1	1.2 ± 0.2	1.4 ± 0.3	1.1 ± 0.1	1.0 ± 0.1	1.3 ± 0.1	0.9 ± 0.3	1.2 ± 0.1	1.3 ± 0.2	1.1 ± 0.3	1.2 ± 0.1
LVEDD (mm)	2.7 ± 0.6	2.9 ± 0.3	3.5 ± 0.1	2.4 ± 0.6	2.6 ± 0.4	3.6 ± 0.5	3.2 ± 0.2	2.5 ± 0.7	3.7 ± 0.3	2.7 ± 0.5	2.8 ± 0.3	3.9 ± 0.2
LVESD (mm)	1.4 ± 0.4	1.6 ± 0.2	2.3 ± 0.2	1.2 ± 0.5	1.7 ± 0.2	2.7 ± 0.7	1.9 ± 0.3	1.8 ± 0.3	2.9 ± 0.3	1.3 ± 0.4	1.9 ± 0.2	3.0 ± 0.2
LVFS (%)	48.5 ± 6.9	45.1 ± 2.8	34.0 ± 3.9	46.2 ± 7.0	30.4 ± 7.7	20.4 ± 2.3	42.7 ± 12.0	31.7 ± 8.1	23.1 ± 4.4	48.9 ± 5.4	32.6 ± 5.8	24.1 ± 4.5
LVEF (%)	81.1 ± 6.9	77.9 ± 3.0	63.9 ± 5.6	78.86 ± 7.5	59.8 ± 11.3	42.3 ± 4.3	73.7 ± 12.7	60.5 ± 11.5	47.0 ± 7.7	81.8 ± 5.1	62.4 ± 7.6	48.3 ± 7.4

Values are shown as mean ± SD. AWd, anterior wall diastole; AWs anterior wall systole; PWd, posterior wall diastole; PWs, posterior wall systole; LVEDD, left ventricle end-diastolic dimension; LVESD, left ventricle end-systolic dimension; LVFS, left ventricle fractional shortening; LVEF, left ventricle ejection fraction; Post-op, post-operation.

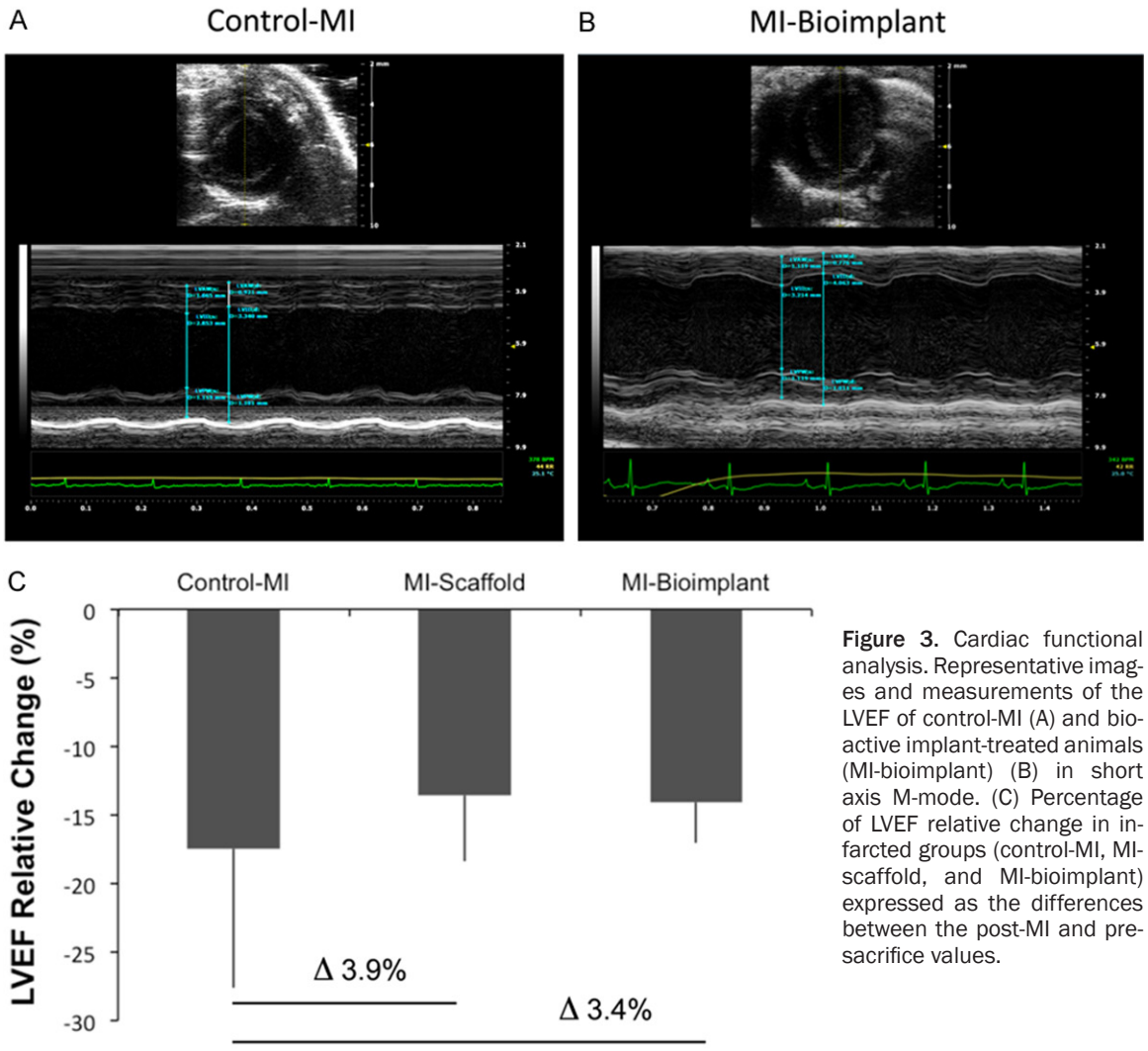

Figure 3. Cardiac functional analysis. Representative images and measurements of the LVEF of control-MI (A) and bioactive implant-treated animals (MI-bioimplant) (B) in short axis M-mode. (C) Percentage of LVEF relative change in infarcted groups (control-MI, MI-scaffold, and MI-bioimplant) expressed as the differences between the post-MI and pre-sacrifice values.

hydrogel (PuraMatrix™) and subATDPCs [23], which display cardiac regenerative capacity. These three components form a bioactive implant that supports implanted cells and provides a hospitable environment for their survival and differentiation. Here we tested the therapeutic efficacy of this bioactive implant in mice, as a preliminary pre-clinical model to assess proof-of-principle.

One of the fundamental aspects of cardiac tissue engineering is to develop a bioprosthesis with a good adaptability to the damaged myocardium. In our experiments, we observed good adaptability of the bioactive implant to the underlying myocardium via macroscopic analysis and histology (**Figure 2**). PCLMA membranes have a comparable resistivity to healthy transmural myocardium (440 Ω and 300-700 Ω of impedance at a pacing pulse of 1 V, 0.5 ms, respectively) [29, 30], suggesting that PCLMA electrical resistivity may facilitate the propagation of electrical pulses throughout the contact area between the bioactive implant and the infarcted zone. Moreover, PCLMA elastomeric membranes support the survival and adhesion of neural cells [31] and articular chondrocytes [21]. Although not all the implanted cells survived in the present investigation, the cardiac environment that they encountered and the properties of the bioactive implant facilitated their differentiation toward cardiac lineages, as reflected by cTnI expression. The PCLMA membrane presents a micropore structure and size (in the 100 μm range) that facilitates the diffusion of nutrients and molecular stimuli from the host tissue to the bioactive implant, enabling the cells to survive and differentiate [21].

Self-assembling peptide hydrogels are synthetic materials that undergo spontaneous assembly into ordered nanostructures [32-34]. Incorporating a self-assembling peptide hydrogel (RAD16-I) into the PCLMA elastomeric membrane improves the characteristics of the bioactive implant in terms of cell survival and differentiation, as demonstrated in previous studies [35-37]. Injection of a self-assembling peptide hydrogel with neonatal rat cardiomyocytes into the rat model of MI previously demonstrated benefits in cardiac function and survival of the injected cells [38]. More importantly, self-assembling peptides also promote differentiation into cardiomyocytes and vascular smooth muscle cells when injected with cardiac progenitors in a mouse MI model [39]. These observations suggest that self-assembling peptide hydrogels are effective for the delivery of various cell types for use in cardiac regeneration therapy. Moreover, when combined with elastomeric membranes, the hydrogel improves cell distribution, facilitating uniform colonization of the membrane pores and cell proliferation [24]. In the present investigation, we also observed uniform distribution of the subATDPCs inside the bioactive implant and differentiation into the cardiac lineage.

Vascularization of the bioactive implant is also important. Interestingly, here the bioimplant was fully vascularized with functional vessels coming from the myocardium, as demonstrated by the presence of FITC-dextran in the lumen of the vessels in the bioactive implant. Proper vascularization is fundamental for cell survival and for integration of the bioprosthesis over the myocardium. Here, channeled scaffolds were produced with the aim to guide the capillary network of the host tissue. Additionally, *in vitro* studies have demonstrated that RAD16-I facilitates the adhesion of endothelial cells, their proliferation, and capillary formation [40, 41]. Moreover, we previously showed that subATDPCS have the capacity to differentiate into the endothelial lineage when implanted over infarcted mouse myocardium [23].

Positive effects on global cardiac motility were observed via echocardiography in the present investigation. We postulate that a paracrine effect comes from the implanted subATDPCs, as previously demonstrated [25]. Also, important gene expression changes were previously found in areas distal from the infarction in dog and swine models, suggesting that the benefits of bioimplants are not only due to local reduction in scar size, but to a more general event [42, 43].

In conclusion, here we propose a new myocardial bioprosthesis consisting of PCLMA elastomeric membrane, RAD16-I peptide hydrogel, and subATDPCs. The membrane provides the shape, stability and mechanical resistance, the RAD16-I peptide hydrogel a suitable cellular microenvironment that mimics the extracellular matrix, enabling cells to survive and differentiate into cardiac lineage. We believe that this bioactive implant is an approximation of a suitable platform for supporting cell delivery over the infarcted myocardium to promote regeneration after ischemic damage.

Acknowledgements

The authors wish to thank the patients who made this study possible and the members of the Department of Cardiac Surgery for their collaboration in obtaining human samples. We also greatly appreciate the contribution of Dr Gálvez-Montón on all statistical analyses. The research leading to these results received funding from the European Union Seventh Framework Programme (Project RECATABI, 7FP/2007-2013) under grant agreement number 229239. This work was also supported by Ministerio de Ciencia e Innovación (SAF2011-30067-C02-01), Fundació La Marató de TV3 (080330), Red de Terapia Celular-TerCel (RD12/0019/0029), Red Cardio-vascular (RD12/0042/0047), Sociedad Española de Cardiología, and Fundació Privada Daniel Bravo Andreu.

Disclosure of conflict of interest

None.

Address correspondence to: Carolina Soler Botija, Heart Failure and Cardiac Regeneration (ICREC) Research Program, Health Research Institute Germans Trias i Pujol (IGTP), Cardiology Service, Hospital Universitari Germans Trias i Pujol, Ctra. de Can Ruti, Camí de les escoles, s/n, 08916 Badalona, Barcelona, Spain. Tel: +34 934978662; Fax: +34 934978654; E-mail: csoler@igtp.cat

References

[1] Olivetti G, Capasso JM, Meggs LG, Sonnenblick EH, Anversa P. Cellular basis of chronic ven-

tricular remodeling after myocardial infarction in rats. Circ Res 1991; 68: 856-869.
[2] Anversa P, Leri A, Kajstura J. Cardiac regeneration. J Am Coll Cardiol 2006; 47: 1769-1776.
[3] Parmacek MS, Epstein JA. Cardiomyocyte renewal. N Engl J Med 2009; 361: 86-88.
[4] Bergmann O, Bhardwaj RD, Bernard S, Zdunek S, Barnabé-Heider F, Walsh S, Zupicich J, Alkass K, Buchholz BA, Druid H, Jovinge S, Frisén J. Evidence for cardiomyocyte renewal in humans. Science 2009; 324: 98-102.
[5] Genovese J, Cortes-Morichetti M, Chachques E, Frati G, Patel A, Chachques JC. Cell based approaches for myocardial regeneration and artificial myocardium. Curr Stem Cell Res Ther 2007; 2: 121-127.
[6] Orlic D, Kajstura J, Chimenti S, Bodine DM, Leri A, Anversa P. Transplanted adult bone marrow cells repair myocardial infarcts in mice. Ann NY Acad Sci 2001; 938: 221-229.
[7] Schuleri KH, Amado LC, Boyle AJ, Centola M, Saliaris AP, Gutman MR, Hatzistergos KE, Oskouei BN, Zimmet JM, Young RG, Heldman AW, Lardo AC, Hare JM. Early improvement in cardiac tissue perfusion due to mesenchymal stem cells. Am J Physiol Heart Circ Physiol 2008; 294: H2002-H2011.
[8] Flynn A, O'Brien T. Stem cell therapy for cardiac disease. Expert Opin Biol Ther 2011; 11: 177-187.
[9] Wollert KC, Meyer GP, Lotz J, Ringes-Lichtenberg S, Lippolt P, Breidenbach C, Fichtner S, Korte T, Hornig B, Messinger D, Arseniev L, Hertenstein B, Ganser A, Drexler H. Intracoronary autologous bone-marrow cell transfer after myocardial infarction: the BOOST randomised controlled clinical trial. Lancet 2004; 364: 141-148.
[10] Kang HJ, Lee HY, Na SH, Chang SA, Park KW, Kim HK, Kim SY, Chang HJ, Lee W, Kang WJ, Koo BK, Kim YJ, Lee DS, Sohn DW, Han KS, Oh BH, Park YB, Kim HS. Differential effect of intracoronary infusion of mobilized peripheral blood stem cells by granulocyte colony- stimulating factor on left ventricular function and remodeling in patients with acute myocardial infarction versus old myocardial infarction. The MAGIC Cell-3-DES randomized, controlled trial. Circulation 2006; 114: I145-51.
[11] Schächinger V, Erbs S, Elsässer A, Haberbosch W, Hambrecht R, Hölschermann H, Yu J, Corti R, Mathey DG, Hamm CW, Süselbeck T, Assmus B, Tonn T, Dimmeler S, Zeiher AM; REPAIR-AMI Investigators. Intracoronary bone marrow-derived progenitor cells in acute myocardial infarction. N Engl J Med 2006; 355: 1210-1221.
[12] Janssens S, Dubois C, Bogaert J, Theunissen K, Deroose C, Desmet W, Kalantzi M, Herbots L, Sinnaeve P, Dens J, Maertens J, Rademakers F, Dymarkowski S, Gheysens O, Van Cleemput J, Bormans G, Nuyts J, Belmans A, Mortelmans L, Boogaerts M, Van de Werf F. Autologous bone marrow-derived stem-cell transfer in patients with ST-segment elevation myocardial infarction: double-blind, randomised controlled trial. Lancet 2006; 367: 113-121.
[13] Leistner DM, Fischer-Rasokat U, Honold J, Seeger FH, Schächinger V, Lehmann R, Martin H, Burck I, Urbich C, Dimmeler S, Zeiher AM, Assmus B. Transplantation of progenitor cells and regeneration enhancement in acute myocardial infarction (TOPCARE-AMI): final 5-year results suggest long-term safety and efficacy. Clin Res Cardiol 2011; 100: 925-934.
[14] Zhang H, Chen H, Wang W, Wei Y, Hu S. Cell survival and redistribution after transplantation into damaged myocardium. J Cell Mol Med 2010; 14: 1078-1082.
[15] Mooney DJ, Vandenburgh H. Cell delivery mechanisms for tissue repair. Cell Stem Cell 2008; 2: 205-213.
[16] Soler-Botija C, Galvez-Monton, C, Prat-Vidal C, Roura S, Bayes-Genis A. Myocardial bioprosthesis: Mimicking nature. Drugs Fut 2013; 38: 475-484.
[17] Vunjak-Novakovic G, Lui KO, Tandon N, Chien KR. Bioengineering heart muscle: a paradigm for regenerative medicine. Annu Pev Biomed Eng 2011; 13: 245-267.
[18] Soler-Botija C, Bago JR, Bayes-Genis A. A bird's-eye view of cell therapy and tissue engineering for cardiac regeneration. Ann N Y Acad Sci 2012; 1254: 57-65.
[19] Gálvez-Montón C, Prat-Vidal C, Roura S, Soler-Botija C, Bayes-Genis A. Cardiac Tissue Engineering and the Bioartificial Heart. Rev Esp Cardiol 2013; 66: 391-399.
[20] Shafy A, Fink T, Zachar V, Lila N, Carpentier A, Chachques JC. Development of cardiac support bioprostheses for ventricular restoration and myocardial regeneration. Eur J Cardiothorac Surg 2013; 43: 1211-1219.
[21] Ivirico JL, Martínez EC, Sánchez MS, Criado IM, Ribelles JL, Pradas MM. Structure and properties of methacrylate-endcapped caprolactone networks with modulated water uptake for biomedical applications. J Biomed Mater Res B Appl Biomater 2007; 83: 266-275.
[22] Léobon B, Roncalli J, Joffre C, Mazo M, Boisson M, Barreau C, Calise D, Arnaud E, André M, Pucéat M, Pénicaud L, Prosper F, Planat-Bénard V, Casteilla L. Adipose-derived cardiomyogenic cells: in vitro expansion and functional improvement in a mouse model of myocardial infarction. Cardiovasc Res 2009; 83: 757-767.
[23] Bagó JR, Soler-Botija C, Casaní L, Aguilar E, Alieva M, Rubio N, Bayes-Genis A, Blanco J.

Bioluminescence imaging of cardiomyogenic and vascular differentiation of cardiac and subcutaneous adipose tissue-derived progenitor cells in fibrin patches in a myocardium infarct model. Int J Cardiol 2013; 69: 288-295.

[24] Vallés-Lluch A, Arnal-Pastor M, Martínez-Ramos C, Vilariño-Feltrer G, Vikingsson L, Castells-Sala C, Semino CE, Monleón Pradas M. Combining self-assembling peptide gels with three-dimensional elastomer scaffolds. Acta Biomater 2013; 9: 9451-9460.

[25] Bayes-Genis A, Soler-Botija C, Farré J, Sepúlveda P, Raya A, Roura S, Prat-Vidal C, Gálvez-Montón C, Montero JA, Büscher D, Izpisúa Belmonte JC. Human progenitor cells derived from cardiac adipose tissue ameliorate myocardial infarction in rodents. J Mol Cell Cardiol 2010; 49: 771-780.

[26] Martinez-Estrada OM, Munoz-Santos Y, Julve J, Reina M, Vilaro S. Human adipose tissue as a source of Flk-1+ cells: new method of differentiation and expansion. Cardiovasc Res 2005; 65: 328-333.

[27] Vilalta M, Jorgensen C, Dégano IR, Chernajovsky Y, Gould D, Noël D, Andrades JA, Becerra J, Rubio N, Blanco J. Dual luciferase labelling for non-invasive bioluminescence imaging of mesenchymal stromal cell chondrogenic differentiation in demineralized bone matrix scaffolds. Biomaterials 2009; 30: 4986-4995.

[28] Kraehenbuehl TP, Langer R, Ferreira LS. Three-dimensional biomaterials for the study of human pluripotent stem cells. Nat Methods 2011; 8: 731-736.

[29] Chachques JC, Pradas MM, Bayes-Genis A, Semino C. Creating the bioartificial myocardium for cardiac repair: challenges and clinical targets. Expert Rev Cardiovasc Ther 2013; 11: 1701-1711.

[30] Salazar Y, Bragos R, Casas O, Cinca J, Rosell J. Transmural versus nontransmural in situ electrical impedance spectrum for healthy, ischemic, and healed myocardium. IEEE Trans Biomed Eng 2004; 51: 1421-1427.

[31] Valdes-Sánchez T, Rodriguez-Jimenez FJ, García-Cruz DM, Escobar-Ivirico JL, Alastrue-Agudo A, Erceg S, Monleón M, Moreno-Manzano V. Methacrylate-endcapped caprolactone and FM19G11 provide a proper niche for spinal cord-derived neural cells. J Tissue Eng Regen Med 2013; [Epub ahead of print].

[32] Zhao X, Zhang S. Self-assembling nanopeptides become a new type of biomaterial. Adv Polym Sci 2006; 203: 145-170.

[33] Quintana L, Fernández Muiños T, Genové E, Olmos MM, Borrós S, Semino CE. Early tissue patterning recreated by mouse embryonic fibroblasts in a three dimensional environment. Tissue Eng Part A 2009; 15: 45-54.

[34] Ortinau S, Schmich J, Block S, Liedmann A, Jonas L, Weiss DG, Helm CA, Rolfs A, Frech MJ. Effect of 3D scaffold formation on differentiation and survival in human neural progenitor cells. Biomed Eng Online 2010; 9: 70.

[35] Thonhoff JR, Lou DI, Jordan PM, Zhao X, Wu P. Compatibility of human fetal neural stem cells with hydrogel biomaterials in vitro. Brain Res 2008; 1187: 42-51.

[36] Castells-Sala C, Sanchez B, Recha-Sancho L, Puig V, Bragos R, Semino CE. Influence of electrical stimulation on 3D-cultures of adipose tissue derived progenitor cells (ATDPCs) behavior. Conf Proc IEEE Eng Med Biol Soc 2012; 2012: 5658-5661.

[37] Cui XJ, Xie H, Wang HJ, Guo HD, Zhang JK, Wang C, Tan YZ. Transplantation of mesenchymal stem cells with self-assembling polypeptide scaffolds is conducive to treating myocardial infarction in rats. Tohoku J Exp Med 2010; 222: 281-289.

[38] Hsieh PC, Davis ME, Gannon J, MacGillivray C, Lee RT. Controlled delivery of PDGF-BB for myocardial protection using injectable self-assembling peptide nanofibers. J Clin Invest 2006; 116: 237-248.

[39] Tokunaga M, Liu ML, Nagai T, Iwanaga K, Matsuura K, Takahashi T, Kanda M, Kondo N, Wang P, Naito AT, Komuro I. Implantation of cardiac progenitor cells using self-assembling peptide improves cardiac function after myocardial infarction. J Mol Cell Card 2010; 49: 972-983.

[40] Genové E, Shen C, Zhang S, Semino CE. The effect of functionalized self-assembling peptide scaffolds on human aortic endothelial cell function. Biomaterials 2005; 26: 3341-3351.

[41] Sieminski AL, Semino CE, Gong H, Kamm RD. Primary sequence of ionic selfassembling peptide gels affects endothelial cell adhesion and capillary morphogenesis. J Biomed Mater Res Part A 2008; 87: 494-504.

[42] Puett DW, Forman MB, Cates CU, Wilson BH, Hande KR, Friesinger GC, Virmani R. Oxypurinol limits myocardial stunning but does not reduce infarct size after reperfusion. Circulation 1987; 76: 678-686.

[43] Prat-Vidal C, Gálvez-Montón C, Nonell L, Puigdecanet E, Astier L, Solé F, Bayes-Genis A. Identification of temporal and region-specific myocardial gene expression patterns in response to infarction in swine. PLoS One 2013; 8: e54785.